

## Two-dimensional waveform analysis in MR elastography of skeletal muscles

Sebastian Papazoglou<sup>1</sup>, Jürgen Braun<sup>2</sup>, Uwe Hamhaber<sup>2</sup> and Ingolf Sack<sup>1</sup>

<sup>1</sup> Institute of Radiology, Charité—University Medicine Berlin, Humboldt University Berlin, Berlin, Germany

<sup>2</sup> Institute of Medical Informatics, Charité—University Medicine Berlin, Free University Berlin, Berlin, Germany

E-mail: [ingolf.sack@charite.de](mailto:ingolf.sack@charite.de)

Received 13 August 2004, in final form 10 December 2004

Published 2 March 2005

Online at [stacks.iop.org/PMB/50/1313](http://stacks.iop.org/PMB/50/1313)

### Abstract

A method for direct determination of anisotropic elastic coefficients using two-dimensional shear wave patterns is introduced. Thereby, the symmetry of the wave patterns is approximated by a squared elliptic equation yielding an explicit relation between waveform and elasticity. The method is used to analyse MR elastography wave images of the biceps acquired by a continuous harmonic excitation at the distal tendon of the muscle. Typically *V*-shaped wave patterns were observed in this type of tissue, which could be well reproduced by the proposed elliptic approximation of the waveform assuming incompressibility and a transverse isotropic model of elasticity. Without additional experiments, the analysis of straightness, slope and interferences of the wave fronts enabled us to deduce two Young's moduli and one shear modulus, which fully describe the anisotropy of the elasticity of muscles. The results suggest strong anisotropy of the living human biceps causing a shear wave speed parallel to the muscle fibres that is approximately four times faster than the perpendicular shear wave speed.

### Introduction

The determination of mechanical properties of human skeletal muscles is of principal interest in medicine and biomechanics (Fung 1993, Humphrey 2002). For this reason elastography techniques have been employed to non-invasively designate mechanical parameters of skeletal muscles under rest or activation (Levinson *et al* 1995, Gao *et al* 1996, Dresner *et al* 2001, Nightingale *et al* 2002, Sack *et al* 2002, Gennisson *et al* 2003, Uffmann *et al* 2004). In dynamic elastography, low frequency shear waves are employed to map the shear modulus in terms of wavelengths of tissue-displacement fields under varying muscle loads (Levinson *et al* 1995, Dresner *et al* 2001, Basford *et al* 2002, Heers *et al* 2003). While in ultrasound

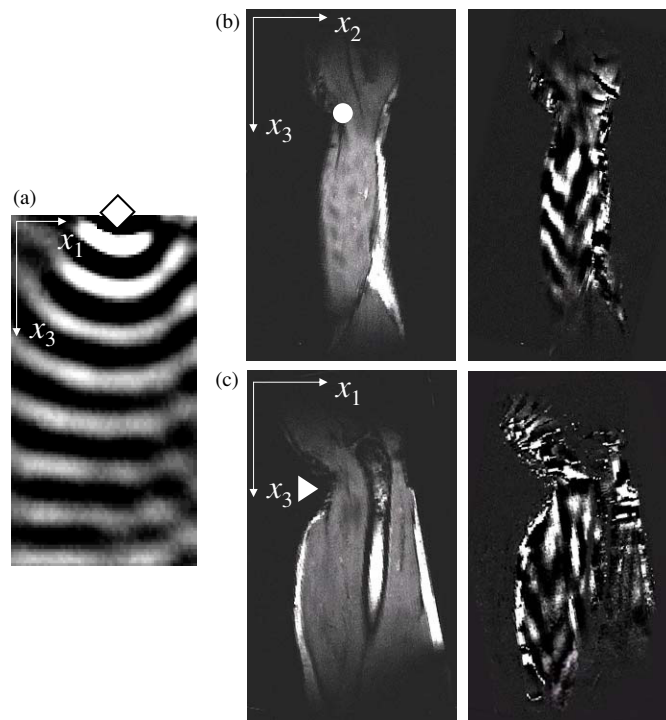


**Figure 1.** Experimental shear waves in agarose (a) and skeletal muscle tissue (b/c). Harmonic shear excitation (200 Hz) was focally introduced in  $x_1$ -direction at positions symbolized by ' $\diamond$ ', ' $\triangleright$ ' and ' $\circ$ ', which also demarcate the origins of the drawn coordinates. The muscle wave images are shown in sagittal (b) and coronal slice position (c) of the right arm of the same volunteer. On the left-hand side of (b) and (c) the magnitudes MRE images are shown that were used for weighting the phase difference signal with the signal magnitude (right-hand side).

elastography the displacement velocity is detected using Doppler techniques (Parker *et al* 1990, Yamakoshi *et al* 1990), in MR elastography (MRE) tissue vibrations are magnetically encoded by oscillating magnetic field gradients (Muthupillai *et al* 1995). Therefore, wave images acquired by MRE reflect specific components of the displacement field corresponding to direction and frequency of the oscillating gradients. The ability of MRE to measure distinct components of the tissue vibration is of particular importance for addressing anisotropy (Sinkus *et al* 2000). Since the direction of wave propagation of the single displacement components is governed by specific elastic moduli, two-dimensional wave images in MRE can reveal the anisotropy of the examined tissue. Thereby, anisotropic properties of the material are directly deducible from wave patterns if (i) the geometry of the excitation source does not restrict the wave propagation and (ii) the boundary conditions are non-reflecting. However, until now MRE has not been employed to directly measure anisotropy from single shear wave images. The purpose of this study was to develop an analytical tool that allows a direct conversion of typical waveforms into anisotropic elastic coefficients. The apparent waveform that is usually displayed in MRE images is a result of the actuator design, the magnetic encoding characteristics during MRE acquisition and the superposition of distinct shear wave modes. The apparent waveform can reflect inherent differences in the elastic properties of the material as demonstrated for agarose and muscle tissue in figure 1. While the waveform in agarose is circular concentric (figure 1(a)) skeletal muscles show tapered

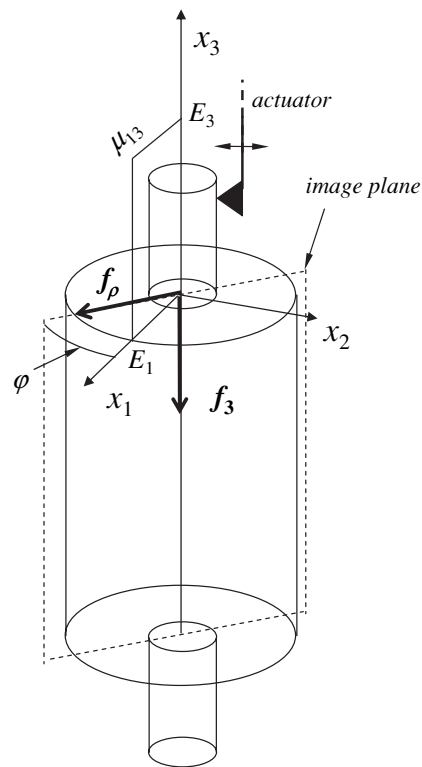


**Figure 2.** Sketch of the biceps with actuator at the distal tendon. The stress and strain components are defined in Cartesian coordinates. As indicated, mechanical excitation in MRE is induced by transverse vibrations of the tendon so that the tangential component  $f_\varphi$  of the resulting force vector becomes zero yielding  $\mathbf{f} = [f_\rho, f_3]^T$ . The image plane is chosen to coincide with the stress plane resulting in a planar stress scenario.

and straight waves (figures 1(b), (c)). Such V-shaped waves were reported by several groups to be characteristic for MRE of skeletal muscle using a mechanical excitation via tendons (Dresner *et al* 2001, Sack *et al* 2002, Uffmann *et al* 2004). Here a waveform analysis is developed, which is appropriate to elucidate anisotropy of soft tissues using two-dimensional MRE wave images. Henceforth, we will describe waveforms in terms of straightness, slope and interferences of the wave fronts. To tackle this goal a two-dimensional, anisotropic elastic model is introduced. Then, the resulting equations of motion are solved in the Fourier space (i.e.  $k$ -space) and a simple formalism is derived to analyse the symmetry of the observed MRE waves in spatial dimensions. The formalism comprises a small set of constraints to elastic coefficients which confine possible elastic scenarios yielding V-waves.

## Theory

### *Transverse isotropic muscle model*

In the following, Cartesian axes are denoted by  $x_i$  ( $i = 1, 2, 3$ ). Our model of transverse isotropy is defined by aligning the principal axis of symmetry  $x_3$  parallel to the muscle fibres (figure 2). Small deformation strain is given by the Green–Lagrange strain tensor ( $\varepsilon_{ij} = 1/2\partial u_j/\partial x_k$ ). According to Hooke’s law the strain tensor  $\varepsilon$  is linearly related to the stress tensor  $\sigma$  by

definition of the rank-four elasticity tensor  $\mathbf{C}$  (using Einstein's summation convention over repeated indices) (Landau and Lifschitz 1986):

$$\sigma_{ij} = C_{ijkl}\varepsilon_{kl}. \quad (1)$$

As shown elsewhere (Lai *et al* 1994), five independent parameters determine the linear elastic properties of a transverse isotropic material: two shear moduli  $\mu_{13} = \mu_{23}$  and  $\mu_{12}$  the Young's modulus  $E_3$  and two Poisson's ratios  $\nu_{31} = \nu_{32}$  and  $\nu_{12}$ . For most biological soft tissues the condition of incompressibility holds in good approximation (Kruse *et al* 2000). In this case the Poisson's ratios are given by

$$\nu_{31} = \frac{1}{2} \quad \nu_{12} = 1 - \frac{1}{2} \frac{E_1}{E_3} \quad (2)$$

and the isotropic shear modulus reads as

$$\mu_{12} = \frac{E_1 E_3}{4E_3 - E_1}. \quad (3)$$

Hence, the elasticity of the muscle can be described by three unknowns:  $E_1$ ,  $E_3$  and  $\mu_{13}$  as assigned in figure 2.

#### *Two-dimensional shear wave propagation*

The equations governing the elastic wave propagation in a homogenous, linear elastic solid comprise three coupled partial differential equations of second order in time and space:

$$\rho \frac{d^2 u_j}{dt^2} - C_{jklm} \frac{\partial^2 u_m}{\partial x_k \partial x_l} = f_j \quad (4)$$

where  $\rho$  is the density of the material,  $u_j$  are the components of the displacement field and  $f_j$  are the components of an external force, e.g. the driving force  $\mathbf{f} = [f_1(\mathbf{x}, t), 0, 0]^T$ . In MRE experiments on skeletal muscles the latter is transmitted from the actuator to the muscle via tendon (figure 2). For reducing the dimensionality of the problem it is assumed that stresses occur solely within planes of symmetry, i.e. planes perpendicular to the  $x_1 x_2$ -plane. As shown in figure 2 this assumption implies that no torsion of the tendon would occur, which was shown to hold in good approximation (Sack *et al* 2003). If the MRE-image plane is chosen so that  $\varphi = 0$  stress components related to  $x_2$  vanish and the elements of the elasticity tensor  $\mathbf{C}$  that correspond to  $x_1$ - and  $x_3$ -strains are given in reduced (Voigt's) notation by

$$C_{11} = 4\mu_{12} = 2C_{13} \quad C_{33} = 4\mu_{12}E_3/E_1 \quad C_{55} = 2\mu_{13}. \quad (5)$$

In this case  $u_2$  uncouples from  $u_1$  and  $u_3$  so that equation (4) can be rewritten as the two-component vector equation

$$\begin{aligned} \rho \frac{\partial^2 \mathbf{u}}{\partial t^2} - \begin{bmatrix} C_{11} & 0 \\ 0 & \mu_{13} \end{bmatrix} \frac{\partial^2 \mathbf{u}}{\partial x_1^2} - \begin{bmatrix} \mu_{13} & 0 \\ 0 & C_{33} \end{bmatrix} \frac{\partial^2 \mathbf{u}}{\partial x_3^2} - \begin{bmatrix} 0 & C_{11}/2 + \mu_{13} \\ \text{sym.} & 0 \end{bmatrix} \frac{\partial^2 \mathbf{u}}{\partial x_3 \partial x_1} \\ = \begin{bmatrix} f_1(x_1, x_3, t) \\ 0 \end{bmatrix} \end{aligned} \quad (6)$$

with  $\mathbf{u} = [u_1(x_1, x_3, t), u_3(x_1, x_3, t)]^T$ . For further proceeding equation (6) is Fourier transformed with respect to the spatial coordinates yielding a system of ordinary differential equations of second order in time:

$$\rho \frac{\partial^2 \hat{\mathbf{u}}}{\partial t^2} + \mathbf{S} \hat{\mathbf{u}} = \begin{bmatrix} \hat{f}_1(k_1, k_3, t) \\ 0 \end{bmatrix}, \quad \text{with } \mathbf{S} = \begin{bmatrix} C_{11}k_1^2 + \mu_{13}k_3^2 & (C_{11}/2 + \mu_{13})k_1k_3 \\ \text{sym.} & \mu_{13}k_1^2 + C_{33}k_3^2 \end{bmatrix}. \quad (7)$$

Here  $\hat{\mathbf{u}}$  denotes the Fourier transformed displacement vector, i.e.  $\hat{\mathbf{u}} = [\hat{u}_1(k_1, k_3, t), \hat{u}_3(k_1, k_3, t)]^T$ , which is related to  $\mathbf{u}$  by the inverse Fourier transform in two dimensions

$$\mathbf{u}(x_1, x_3, t) = \frac{1}{(2\pi)^2} \int_{-\infty}^{\infty} \int_{-\infty}^{\infty} \hat{\mathbf{u}}(k_1, k_3, t) e^{i(k_1 \cdot x_1 + k_3 \cdot x_3)} dk_1 dk_3. \quad (8)$$

Henceforth, we will restrict our attention to the waveform analysis of  $u_1$ , which was measured in our MRE experiments as depicted in figure 1. Assuming a  $\delta$ -like excitation  $u_1(x_1 = 0, x_3 = 0)$  at time  $t = 0$  the initial value problem is solved by

$$\hat{u}_1 = a_1(e^{i\omega_1 t} + e^{-i\omega_1 t}) + a_2(e^{i\omega_2 t} + e^{-i\omega_2 t}), \quad (9)$$

with

$$\omega_{1,2} = \frac{1}{\sqrt{2\rho}} \sqrt{S_{11} + S_{22} \pm \xi} \quad \text{and} \quad a_{1,2} = \pm \frac{(S_{11} - S_{22})}{4\xi} + \frac{1}{4}, \quad (10)$$

$$\xi = \sqrt{(S_{11} - S_{22})^2 + 4S_{12}^2}.$$

The eigenvalues of  $\mathbf{S}$  are the angular frequencies  $\omega_{1,2}$  of two plane wave modes, a fast (FT) and a slow transverse mode (ST), modulated by  $a_1$  and  $a_2$ , respectively. The lines of constant frequency  $\omega_{1,2} = 2\pi f_v$  ( $f_v =$  vibration frequency) describe closed curves, which represent the waveform in  $k$ -space. Figure 3 exemplary shows the angular frequencies  $\omega_{1,2}$  for three different constitutive ratios  $C_{11}/\mu_{13}$  and  $C_{33}/\mu_{13}$  that provide a measure for the anisotropy of the material. For an isotropic, incompressible medium Hooke's law yields  $C_{11}/\mu_{13} = C_{33}/\mu_{13} = 4$ . Transverse isotropy abolishes all constrains of  $C_{11}$  and  $C_{33}$  with respect to  $\mu_{13}$ . However,  $C_{33}$  is assumed to be at least greater than  $C_{11}/4$  for ensuring  $E_3 > 0$  (see equation (5)).

#### *Elliptic approximation of the waveform*

The apparent form of the shear waves observed in MRE experiments is determined by the superposition of the FT and ST wave modes (equation (9)) transformed back into spatial coordinates using equation (8). Therefore, analysing the waveform requires an expression that accounts for the geometry of both wave modes in spatial coordinates. To tackle this goal the forth-order equations  $\omega_{1,2}$  were approximated by second-order equations yielding a single apparent wave mode. In this approach the coefficients  $e_i$  of a squared elliptic equation,

$$(e_1 k_1^2 + 2e_2 k_1 k_3 + e_3 k_3^2 + 2e_4 k_1 + 2e_5 k_3 + e_6)^2 = 0, \quad (11)$$

are compared to the elastic coefficients of  $\omega_{1,2}$  (equation (10)). This procedure yields 8 distinct ellipses with coefficients

$$\begin{aligned} e_1 &= 2\sqrt{C_{11}\mu_{13}} \\ e_2 &= \pm\sqrt{|C_{33}\mu_{13} + C_{11}^2/4 + 2\mu_{13}\sqrt{C_{11}C_{33}} - C_{11}C_{33}|} \\ e_3 &= 2\sqrt{C_{33}\mu_{13}} \\ e_4 &= \pm\omega\sqrt{\rho}\sqrt{\mu_{13} + C_{11} - 2\sqrt{C_{11}\mu_{13}}} \\ e_5 &= \pm\omega\sqrt{\rho}\sqrt{\mu_{13} + C_{33} - 2\sqrt{C_{33}\mu_{13}}} \\ e_6 &= -2\omega^2\rho \end{aligned} \quad (12)$$

as displayed in figure 3 for different anisotropic elasticities. The signs of the roots are chosen to obtain real ellipses. The waveform in  $k$ -space is now ascribed to superposed ellipses whereby a translation of the ellipses along  $k_1$  and  $k_3$  shall be neglected for further proceeding. This simplification implies that  $e_4 = e_5 = 0$  and thus, two ellipses remain, which express the

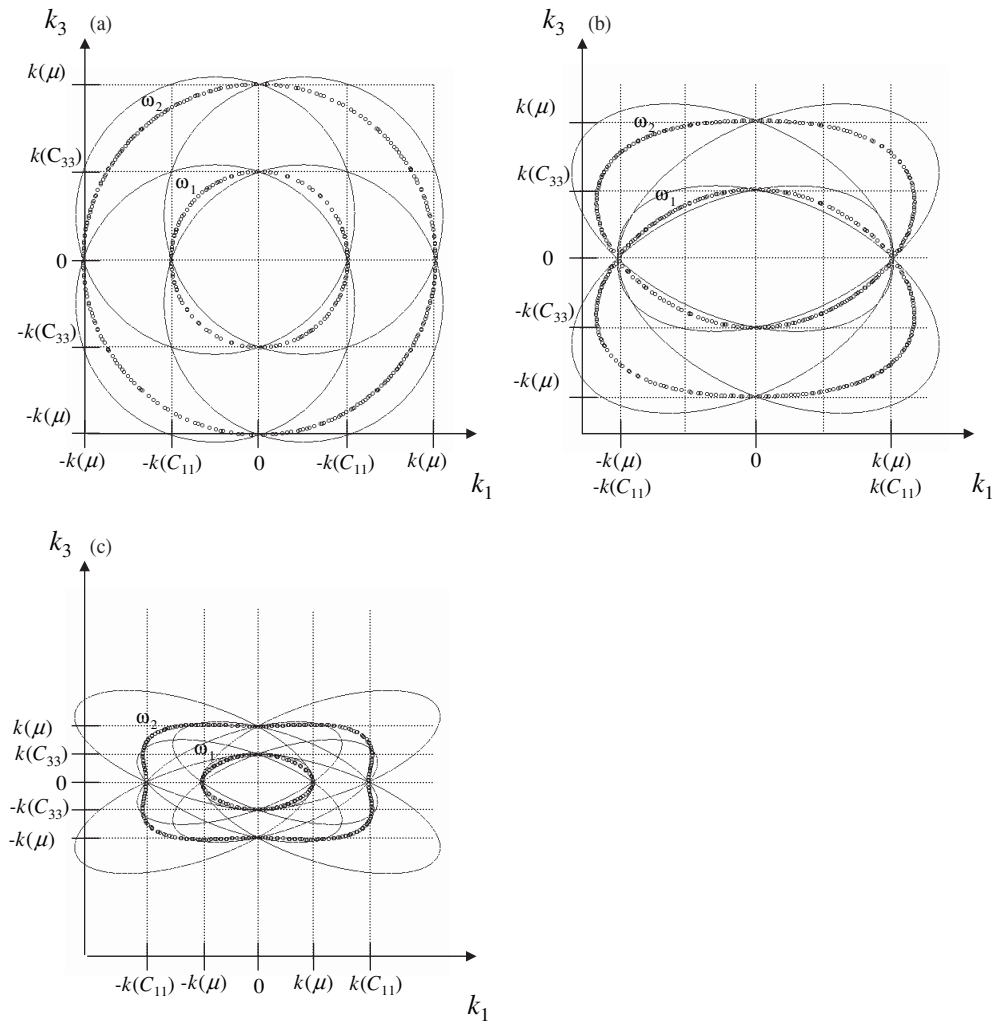


**Figure 3.** Implicit plot of  $\omega(k_1, k_3)$ . The material is assumed to be incompressible ( $\nu_{31} = 1/2$ ) and the ratio  $C_{33}/\mu_{13}$  is fixed to 4 (isotropic relation), whereas  $C_{11}/\mu_{13}$  is varied with 4 (a), 1 (b) and 1/4 (c). The full fourth-order equation (equation (10)) yields the scattered (o) plots, while the elliptic roots (equations (11), (12)) are shown as line graphs. Tick marks:  $k(\mu) = \omega\sqrt{\rho/\mu_{13}}$ ,  $k(C_{11}) = \omega\sqrt{\rho/C_{11}}$  and  $k(C_{33}) = \omega\sqrt{\rho/C_{33}}$ .

geometry of the apparent wave in terms of their axis ratio

$$R = r_1/r_2 \quad \text{with} \quad r_{1,2} = e_1 + e_3 \pm \sqrt{(e_1 - e_3)^2 + 4e_2^2} \quad (13)$$

and the tilt angle  $\alpha_e = \arctan 2e_2/(e_1 - e_3)$  (figure 4(c)). Since the symmetry is conserved during Fourier transformation (equation (8)) the elliptic approximation can be used for geometrical considerations of the waveform also in spatial coordinates. An analytic expression for the  $V$ -angle (henceforth denoted as  $\alpha_V$ ) can be deduced from the ratio of the intercepts of the ellipses at the  $x_1$ - and  $x_3$ -axis (figure 5(c)):

$$\alpha_V = 2 \arctan \left[ \left( \frac{E_1}{E_3} \right)^{\frac{1}{4}} \right]. \quad (14)$$

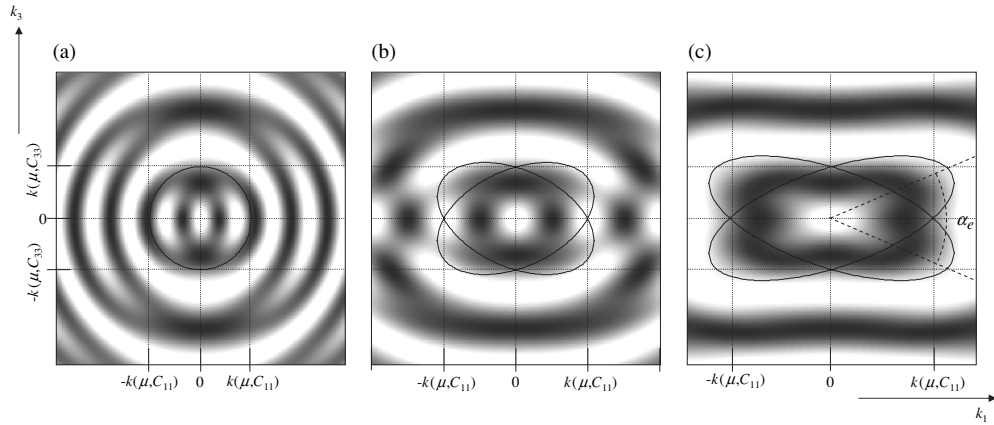


**Figure 4.**  $\hat{u}_1$  wave images calculated using equation (9) and the ratios  $C_{11}/\mu_{13} = 4$  (a), 1 (b), 1/4 (c) and  $C_{33}/\mu_{13} = 4$ . The elliptic approximations for  $\omega_1$  and  $\omega_2$  ( $e_4 = e_5 = 0$ , see equations (11), (12)) are superposed as line graphs.  $\alpha_e$  defines the elliptic rotation angle. Tick marks:  $k(\mu, C_{11}) = \omega\sqrt{\rho/\sqrt{\mu_{13}C_{11}}}$ ,  $k(\mu, C_{33}) = \omega\sqrt{\rho/\sqrt{\mu_{13}C_{33}}}$ .

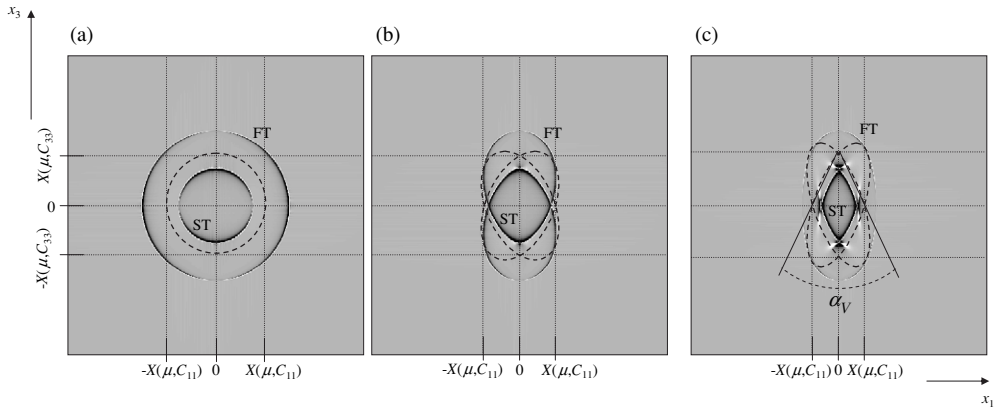


**Figure 5.** Real parts of  $u_1$ -waves calculated with  $C_{11}/\mu_{13} = 4$  (a), 1 (b), 1/4 (c) and  $C_{33}/\mu_{13} = 4$ .  $\alpha_V$  is used to define the apparent  $V$ -angle (equation (15)). The axes labels refer to the positions  $X(\mu, C_{11}) = \sqrt{\mu_{13}C_{11}/\rho}/\omega$  or  $X(\mu, C_{33}) = \sqrt{\mu_{13}C_{33}/\rho}/\omega$ .

This holds for  $R \gg 1$ , i.e. the branches of the ellipses enclosing  $\alpha_V$  can be approximated by straight lines. From this condition certain constraints for the deducibility of  $\alpha_V$  arise according to the straightness of the wave fronts.

In the case of anisotropy the wave vector  $\mathbf{k}$  and the corresponding group velocity  $\mathbf{c} = \partial\omega(\mathbf{k})/\partial\mathbf{k}$  are not necessarily collinear so that interferences of plane waves may appear (Taylor *et al* 1969, Salo and Salomaa 2003). Figure 6 shows the projection of  $\mathbf{c}$  and  $\mathbf{k}$  onto the  $k_1$ -axis, which shows that the direction of wave propagation is increasingly different from the wave normals with increasing anisotropy. An estimate of the degree of such internal interferences can be derived from the elliptic approximation by consideration of the tilt of the ellipses  $\alpha_e$  and the elliptic aspect ration  $R$ :

$$R' = R \tan(\alpha_e/2), \tag{15}$$

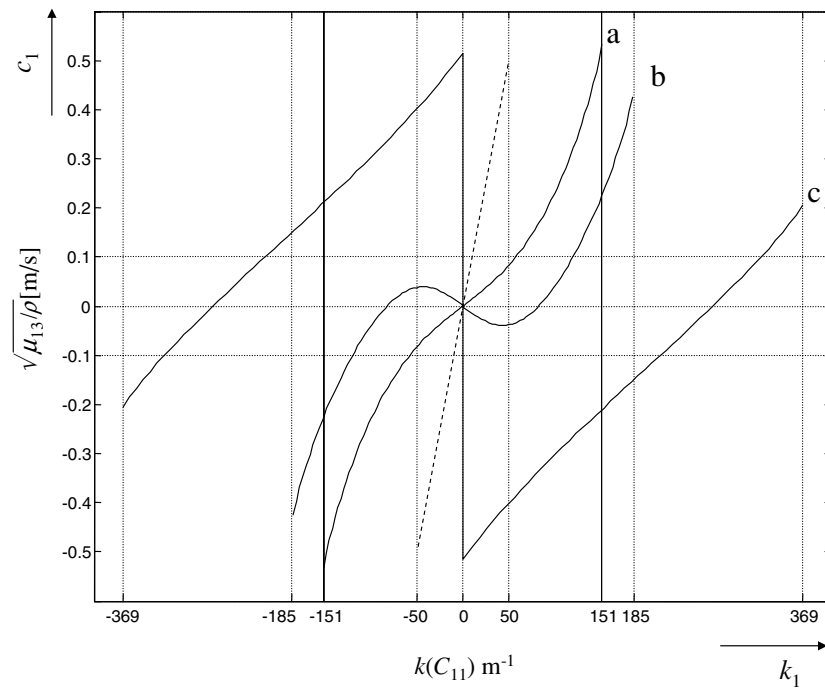


**Figure 6.**  $x_1$ -component of the wave speed  $c_1 = \partial\omega_2(k_1, k_3)/\partial k_1$  versus  $k_1$  with  $k_3$ -values derived from equation (10). The calculations of graphs (a)–(c) correspond to the elastic ratios used in figures 5(a)–(c). The  $k_1$ -ticks correspond to  $\omega = 100$  Hz,  $\rho = 1.1$  kg l $^{-1}$ . It is visible that decreasing ratios  $C_{11}/\mu_{13}$  and  $C_{33}/\mu_{13}$  cause a growing fraction of  $c_1$  that is inverse relative to the sign of  $k_1$ . A negative component of  $c_1$  yields interferences since forward and backward running waves cross each other. The dashed line indicates the isotropic scenario, i.e. circular propagating waves.

i.e. the main axes of the ellipses are projected on  $k_1$  and weighted by  $R$ . In spatial coordinates this provides an estimate of the directionality of the  $c_1$ -component relative to  $k_1$ .

Now, the determination of the anisotropic elastic coefficients can proceed as follows: the wavelength on the  $x_3$ -axis in the  $u_1$  image directly delivers the shear modulus  $\mu_{13}$ . This is the measurement commonly used in MRE. The second measurement is the  $V$ -angle  $\alpha_V$ , that determines the ratio  $E_1/E_3$ . Additionally, the conditions of straightness ( $R$ ) and interferences ( $R'$ ) confine the possible constitutive ratios  $C_{11}/\mu_{13}$  and  $C_{33}/\mu_{13}$ .

## Methods

MRE experiments were performed on a 1.5 T scanner (Siemens Magnetom Vision, Erlangen, Germany). Physical coordinates were assigned to the scanner system with  $x_1$ : l  $\rightarrow$  r,  $x_2$ : a  $\rightarrow$  p and  $x_3$ : h  $\rightarrow$  f. For inducing shear vibrations in  $x_1$ -direction in agarose (1.5% in water) an actuator was designed that allowed a main shear deflection perpendicular to the  $B_0$ -field (Braun 2003). For data acquisition a modified echo planar imaging sequence was used (Braun 2002) (TR: 2 s; TE: 113 ms; FoV: 220 mm; matrix size: 96  $\times$  128). The actuation of the biceps was achieved by a rocker unit with electromotive coil. The device was mounted at the distal biceps tendon of one volunteer and adjusted to vibrate in  $x_1$ -direction. Here the data were acquired using a modified gradient echo imaging sequence (TR: 60 ms; TE = 12 ms;

FoV: 320 mm  $\times$  160 mm; matrix size: 256  $\times$  128). For mechanically exciting both phantom and muscle 7 cycles of 200 Hz oscillations were applied. Motion encoding was achieved by two trapezoidal gradient cycles (200 Hz) applied in  $x_1$ -direction. Two images with inverse oscillating gradients were recorded in one experiment for subtracting corresponding phase images to eliminate static phase shifts.

Profiles along the  $x_3$ -axis of the wave images were used to determine the shear modulus  $\mu_{13}$  by the wavelength  $\lambda_3 = \sqrt{\mu_{13}/\rho}/f_v$  (Dresner *et al* 2001). Wave simulations were performed using the approach of coupled harmonic oscillators for solving equation (6) (Braun *et al* 2001). A finite difference scheme was developed incorporating non-reflecting boundary conditions (Sommerfeld radiation conditions) and a local (harmonic) excitation in  $x_1$ -direction at the center of the upper boundary of a 100  $\times$  200 matrix. Simulations were performed using Matlab<sup>®</sup>R13 (The MathWorks, Natick, MA, USA). Computation time was 21 s on a Pentium IV 2.6 GHz computer.

## Results

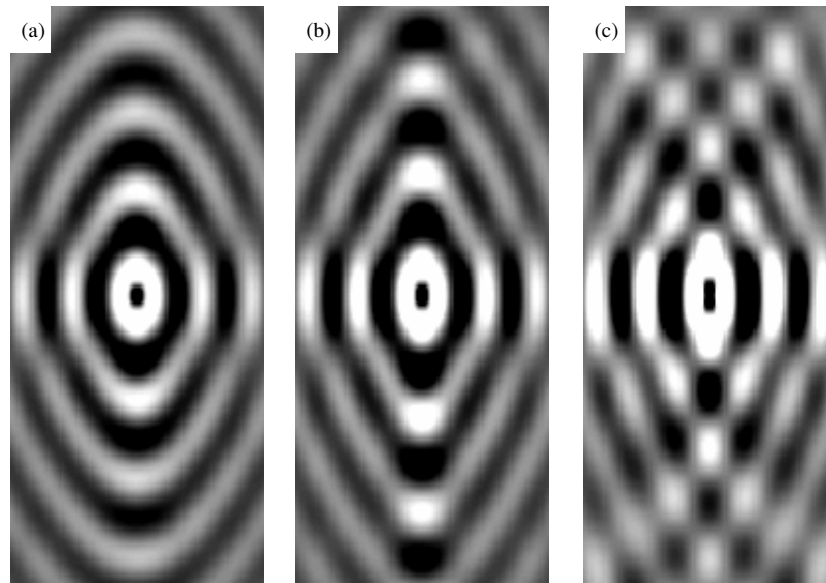
### *MRE experiments*

Figure 1 shows typical MRE-shear waves in agarose and human biceps induced by a focal transducer. It is well visible that in agarose the shear waves emanate in a concentric-circular pattern from the actuator, while in muscles  $V$ -waves appear travelling along  $x_3$  through the biceps. The image plane can be rotated around  $x_3$  without changing the  $V$ -shape of the shear waves, which is experimentally demonstrated by changing the sagittal image plane (figure 1(b)) to be in a coronal position (figure 1(c)).  $\alpha_V$  was estimated with  $55^\circ$  corresponding to former studies (Sack *et al* 2002, 2003). The shear modulus  $\mu_{13}$  was found to be  $54 \pm 3$  kPa for both coronal and sagittal slice positions of the biceps and  $8.6 \pm 0.2$  kPa for the isotropic phantom.

### *Finite difference simulations*

Figure 7 shows three  $u_1$ -wave images calculated using elastic parameters  $C_{11}$ ,  $C_{33}$  and  $\mu_{13}$  that fit to the experimentally deduced angle  $\alpha_V = 55^\circ$ . It is visible that the straightness of the wave fronts is a crucial parameter to determine elasticity. While the waves in figure 7a show circular cusps and wave fronts, figures 7(b), (c) display rather straight and tapered wave fronts, which allow the determination of  $\alpha_V$ . The aspect ratio  $R$  (equation (13)) was determined with 5, 6.4 and 9.9, for figures 7(a), (b) and (c) respectively. Additional variations of  $R$  from 1 (corresponding to isotropy, i.e. circular waves as shown in the experiment of figure 1(a)) to 10 revealed an approximate threshold of 6 for discriminating between circular and straight wave fronts. This eye-guided estimate indicates that for small  $R$ -value equation (13) becomes obsolete since the observed wave shape is no longer represented by  $V$ -waves and thus, no  $\alpha_V$  exists.

Moreover, finite difference simulations revealed the influence of internal interferences to the apparent waveform. Such distortions of  $V$ -waves are clearly visible in figure 7(c). Since in MRE experiments, no such pronounced interferences were found certain combinations of  $C_{11}$ ,  $C_{33}$  and  $\mu_{13}$  could be excluded. The wave images figures 7(a)–(c) corresponding to  $R' = 1.4$ , 2.2 and 4.1, respectively, demonstrate that beyond a certain threshold of  $R'$  internal interferences dominate the apparent waveform. This empirical threshold was found to be  $R' = 3$  which is equal to an inverse  $c_1$ -component (relative to  $k_1$ ) of 0.1 (figure 6). Figure 8 shows how the ‘upper’ ( $R$ ) and ‘lower’ ( $R'$ ) margins of  $C_{11}/\mu_{13}$  and  $C_{33}/\mu_{13}$  apply for



**Figure 7.** Finite difference simulations of  $u_1$ -waves applying a hypothetical  $x_1$ -excitation at the image centre. The simulation parameters were chosen to constrain  $\alpha_V \approx 55^\circ$  with  $C_{11}/\mu_{13} = 0.4406$ ,  $C_{33}/\mu_{13} = 6$  (a);  $C_{11}/\mu_{13} = 0.2937$ ,  $C_{33}/\mu_{13} = 4$  (b);  $C_{11}/\mu_{13} = 0.0734$ ,  $C_{33}/\mu_{13} = 1$  (c).

estimating the occurrence of  $V$ -waves. The grey patch indicates elastic ratios that yield  $V$ -waves, while the fat solid line corresponds to  $\alpha_V = 55^\circ$ . The conjunction of both criteria allowed the determination of the elastic ratios  $C_{11}/\mu_{13} = 0.25 \pm 0.07$  and  $C_{33}/\mu_{13} = 3.4 \pm 1.0$  for the biceps. Using the experimental shear modulus  $\mu_{13}$ ,  $C_{11}$  was derived with  $13.5 \pm 4.5$  kPa and  $C_{33}$  with  $190 \pm 60$  kPa, yielding  $\mu_{12}$ ,  $E_1$  and  $E_3$  with  $3.4 \pm 1.1$ ,  $13 \pm 4.5$  and  $185 \pm 60$  kPa, respectively. Assuming a density of muscle tissue of approximately 1.1 kg/l the shear wave speeds perpendicular and parallel to the muscle fibres followed with  $1.76 \pm 0.03$  m/s and  $7 \pm 1.65$  m/s, respectively. Thus, the ratio between these two shear wave speeds is about 1 to 4.

## Discussion

The experiments show that MRE shear wave patterns convey information about the anisotropy of the material. Corresponding to previous MRE studies (Dresner *et al* 2001, Sack *et al* 2002, Uffmann *et al* 2004) it is found that the apparent waveform observed in anisotropic muscle tissue significantly differs from the waveform in agarose. Opposed to concentric circular waves in isotropic materials, the anisotropy of skeletal muscles yields typical  $V$ -waves in MRE experiments. The anisotropy of muscles can be modelled by transverse isotropy, which is supported by the experiments shown in figures 1(b), (c). There, it is visible that a rotation of the image plane around the main axis of the muscle does not change principle characteristics of  $V$ -waves. The conclusion about the presence of cylindrically symmetric waves from 2D-MRE images is still an assumption, however, considering muscle shape, fibre direction and a focal excitation the cone remains the most compelling 3D-wave shape in muscles since the original discovery of  $V$ -waves by MRE (Dresner *et al* 2001). It was shown that such a  $V$ -waveform arises independently of the wavelength  $\lambda_3$ , implying that the stiffness of the

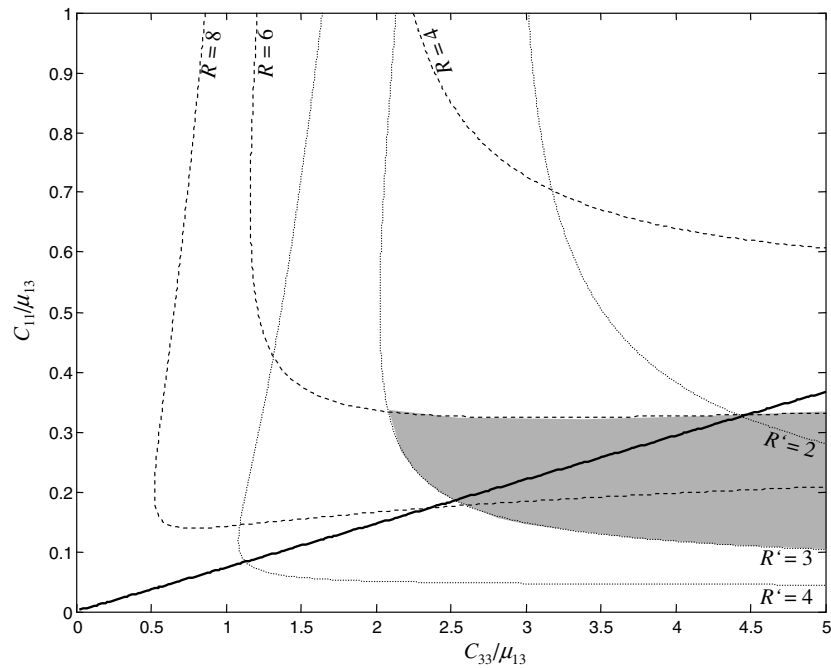


**Figure 8.** Contours of  $R$  and  $R'$  dependent on the constitutive ratios  $C_{11}/\mu_{13}$  and  $C_{33}/\mu_{13}$ . The isolines  $R = 6$  and  $R' = 3$  are used as thresholds enclosing the area of possible ratios where  $V$ -waves appear (grey patch). The fat solid line gives all constitutive ratios that yield an apparent  $V$ -angle  $\alpha_V = 55^\circ$ .

muscle due to muscle load does not influence the waveform. Further, equal  $V$ -wave patterns with an equal angle  $\alpha_V$  were found among different individuals as shown in (Sack *et al* 2002). Also in muscles other than the biceps tapered patterns have been observed (data not shown), which were, however, more convoluted and superposed due to overlaid and less separated muscle groups. This indicates that living human skeletal muscles impose characteristic wave patterns due to characteristic symmetries of the elasticity tensor. However, the occurrence of  $V$ -waves is restricted to non-reflecting boundary conditions as well as an excitation via tendon. The relationship between shape of the excitation source and the resulting waveform in muscles was previously demonstrated (Sack *et al* 2002). If the waves are introduced focally the waveform is governed by elastic properties of the material rather than shape and surface pressure of the actuator. Then, the proposed waveform analysis is feasible. Since it is based on a two-dimensional description of the wave propagation it can directly be applied to MRE waves, which are commonly acquired as 2D-image slices. The used simplification of planar stresses is justified for a cylinder symmetrical problem if the torsion component of the acting force ( $f_\varphi$ ) is zero and the analysed waveform does not depend on the rotation of the image plane. This model allows us to derive simple analytical expressions for the 2D-waveform as well as to implement a finite difference scheme to solve the equation of motion with reasonable resolution. The assumption of planar stresses is obsolete if the actuator produced torsion of the tendon or the image plane was off-centred within the muscle.

The plane stress model reveals two wave modes with different wave speeds that are superposed in the apparent waveform in MRE. Each mode governs the wave propagation along different directions with respect to the vibration direction of the source. Considering an

$x_1x_3$ -image plane a transverse vibration of the biceps tendon constrains pure radial excitation in  $x_1$ -direction. With an alignment of vibration and motion encoding, as commonly applied in MRE, the  $u_1$ -displacement field reflects the experimental findings. The propagation of this component of  $\mathbf{u}$  through an anisotropic medium is well described in  $k$ -space by equation (9). The angular frequencies  $\omega_{1,2}$  describe different waveforms of the FT and ST mode in an anisotropic elastic tissue (figure 3). As an expression of a mean wave mode the application of an elliptic equation with coefficients  $e_1$ ,  $e_2$ ,  $e_3$  and  $e_6$  (equation (12)) was proposed. As a result two conversely rotated ellipses are obtained whose intercepts of the axes precisely describe the geometric mean of the FT and ST wave modes. Thus, for the elastic scenario where  $C_{11}$ ,  $C_{33}$  and  $\mu_{13}$  are equal to each other the proposed elliptic expression coincides with the full  $\omega_{1,2}$ -solution. For arbitrary combinations of these elastic coefficients the ellipses approximate fast and slow running shear waves as a single mean shear wave that conveys the entire elastic information. This important property of the elliptic approximation enables us to estimate the coefficient  $E_3$  that is not accessible by axial wave profiles (along  $x_1$  and  $x_3$ ) taken from  $u_1$ -wave images. Furthermore, in anisotropic media  $C_{11}$  and  $\mu_{13}$  are not necessarily related to the axial wavelengths  $\lambda_1$  and  $\lambda_3$ . In the presence of internal interferences ( $R' < 3$ ) these profiles could reveal a shorter apparent wavelength and thus, both  $C_{11}$  and  $\mu_{13}$  are underestimated. Also considering the proportions of the biceps, it is often difficult to evaluate wave lengths along the short axis of an oblong object. The elliptic approximation is capable of yielding the ratios  $C_{11}/\mu_{13}$  and  $C_{33}/\mu_{13}$ , by simply considering a specific apparent waveform. In the case of  $V$ -waves the elastic parameters that afford this unique waveform are limited to a confined area in the contour plot of figure 8. The thresholds  $R$  and  $R'$  that determine the range of possible elastic coefficients are derived from considerations about the straightness of the wave fronts and the degree of internal interferences. Both criteria were found by simulations to be the simplest and most objective waveform-parameters that can predict the occurrence of  $V$ -waves in terms of  $E_1$ ,  $E_2$  and  $\mu_{13}$ . Although the empirically found thresholds of  $R > 6$  and  $R' > 3$  do not express analytical limits, they provide a practical means to immediately conclude about the probable elasticity behind  $V$ -waves. Therefore, the important information carried by the wave images in figures 1(b) and c is the  $V$ -waveform itself that is found in human skeletal muscles. The specific angle  $\alpha_V$  displays a means to further refine the possible elastic parameters indicating that the shear wave speed parallel to the muscle fibres is about four times faster than perpendicular to them. The same directional dependence of the shear wave speed was found by Gennisson *et al* (2003) using an ultrasound transducer. There, multiple experiments with variable directions of the shear wave source revealed different wave velocities. The agreement of those directly measured quantities and the wave speeds gained by the proposed waveform analysis demonstrates the feasibility of the new method to investigate anisotropic soft tissues by MRE. Since  $V$ -waves can be observed in MRE experiments on different skeletal muscles the underlying type of elasticity seems to be well accessible by analysing the waveform. This offers prospect for the future to use two dimensional shear wave patterns for analysing three-dimensional fibre structures and elastic properties of more complex muscles than the biceps.

## Conclusion

Characteristic two-dimensional shear wave patterns in MRE can be analysed to reveal the anisotropy of the material. A solution of the governing equations of motion based on a planar stress scenario allows specifying the elastic coefficients of the material depending on the apparent waveform in MRE. The algorithm outlined above employs an elliptic approximation of slow and fast transverse wave modes in order to quantify straightness and interferences of

shear wave patterns. Both criteria, applied for the determination of the anisotropy of elasticity in living human biceps, revealed a ratio of 1:4 between the shear wave speeds perpendicular and parallel to the muscle fibres. This demonstrates that even a simple visual estimate of the presence of specific *V*-waves can provide valuable information about the elasticity of the tissue. The proposed waveform analysis can be applied to all elastography techniques, which capture polarized shear wave fields in incompressible soft tissue.

### Acknowledgments

The authors would like to thank Dr Gerd Buntkowsky for stimulating discussions. Financial support of the German Research Foundation (DFG) is gratefully acknowledged (grant Sa 901/3-1).

### References

- Basford J R *et al* 2002 Evaluation of healthy and diseased muscle with magnetic resonance elastography *Arch. Phys. Med. Rehabil.* **83** 1530–6
- Braun J *et al* 2001 Simulation and analysis of magnetic resonance elastography wave images using coupled harmonic oscillators and gaussian local frequency estimation *Magn. Reson. Imaging* **19** 703–13
- Braun J *et al* 2002 In vivo magnetic resonance elastography of the human brain using ultrafast acquisition techniques *Proc 10th Annual Meeting ISMRM (Honolulu)*
- Braun J *et al* 2003 An electromagnetic actuator for generating variably oriented shear waves in MR elastography *Magn. Reson. Med.* **50** 220–2
- Dresner M A *et al* 2001 Magnetic resonance elastography of skeletal muscle. *J. Magn. Reson. Imaging* **13** 269–76
- Fung Y 1993 *Biomechanics: Mechanical Properties of Living Tissue* (New York: Springer)
- Gao L *et al* 1996 Imaging of the elastic properties of tissue—a review *Ultrasound Med. Biol.* **22** 959–77
- Gennisson J L *et al* 2003 Transient elastography in anisotropic medium: application to the measurement of slow and fast shear wave speeds in muscles *J. Acoust. Soc. Am.* **114** 536–41
- Heers G *et al* 2003 Measurement of muscle activity with magnetic resonance elastography *Clin. Biomech (Bristol, Avon)* **18** 537–42
- Humphrey J D 2002 Continuum biomechanics of soft biological tissues *Proc. R. Soc. Lond. A Mat.* **459** 3–46
- Kruse S A *et al* 2000 Tissue characterization using magnetic resonance elastography: preliminary results *Phys. Med. Biol.* **45** 1579–90
- Lai W M *et al* 1994 *Introduction to Continuum Mechanics* (Oxford: Butterworth-Heinemann Ltd)
- Landau L D and Lifschitz E M 1986 *Theory of elasticity* (Oxford: Pergamon Press)
- Levinson S F *et al* 1995 Sonoelastic determination of human skeletal muscle elasticity *J Biomech* **28** 1145–54
- Muthupillai R *et al* 1995 Magnetic resonance elastography by direct visualization of propagating acoustic strain waves *Science* **269** 1854–7
- Nightingale K *et al* 2002 Acoustic radiation force impulse imaging of in vivo vastus medialis muscle under varying isometric load *Ultrasound Imaging* **24** 100–8
- Parker K J *et al* 1990 Tissue response to mechanical vibrations for sonoelasticity imaging *Ultrasound Med. Biol.* **16** 241–6
- Sack I *et al* 2002 Analysis of wave patterns in MR elastography of skeletal muscle using coupled harmonic oscillator simulations *Magn. Reson. Imaging.* **20** 95–104
- Sack I *et al* 2003 Simulation of in vivo MR Elastography wave patterns of skeletal muscles using a transverse isotropic elasticity model *Proc 11th Annual Meeting ISMRM (Toronto)*
- Salo J and Salomaa M M 2003 Nondiffracting waves in anisotropic media *Phys. Rev. E* **67** 056609
- Sinkus R *et al* 2000 High-resolution tensor MR elastography for breast tumour detection *Phys. Med. Biol.* **45** 1649–1664
- Taylor B *et al* 1969 Phonon focusing in solids *Phys. Rev. Lett.* **23** 416–9
- Uffmann K *et al* 2004 In vivo elasticity measurements of extremity skeletal muscle with MR elastography *NMR Biomed* **17** 181–90
- Yamakoshi Y *et al* 1990 Ultrasonic imaging of internal vibration of soft tissue under forced vibrations *IEEE Trans. Ultrason. Ferroelectr. Freq. Control* **37** 45–53